

Article

An Integrated Approach for Urban Pluvial Flood Risk Assessment at Catchment Level

Man Qi ¹, Huabing Huang ² , Lin Liu ¹ and Xi Chen ^{1,*}

¹ Department of Geography and Geographic Information Science, University of Cincinnati, Cincinnati, OH 45221, USA; qimn@mail.uc.edu (M.Q.); liuln@ucmail.uc.edu (L.L.)

² School of Geography and Planning, Sun Yat-sen University, Guangzhou 510275, China; huanghb7@mail.sysu.edu.cn

* Correspondence: chen2x6@ucmail.uc.edu

Abstract: With the rapid development of urbanization and global climate change, urban pluvial floods have occurred more frequently in urban areas. Despite of the increasing urban pluvial flood risk, there is still a lack of comprehensive understanding of the physical and social influencing factors on the process. To fill this knowledge gap, this paper proposes a novel approach to calculate the comprehensive urban pluvial flooding risk index (PFRI) and investigates the interplay impacts from different components at catchment level. To be more specific, PFRI is determined by two components, Exposure Index (EI) and Social Vulnerability Index (SoVI). EI is evaluated based on two indicators, the depression-based Topographic Control Index (TCI) and impervious area ratio. SoVI is measured based on a set of demographic and socio-economic indicators. Our results demonstrated the spatial heterogeneity of urban pluvial flood exposure and social vulnerability, as well as the composite flooding risk across the study area. Our catchment-based urban pluvial flooding risk assessment method can provide a comprehensive understanding of urban flooding and promote the formulation of effective flood mitigation strategies from the catchment perspective.

Keywords: urban pluvial flooding; flood exposure; social vulnerability; topographic control index



Citation: Qi, M.; Huang, H.; Liu, L.; Chen, X. An Integrated Approach for Urban Pluvial Flood Risk Assessment at Catchment Level. *Water* **2022**, *14*, 2000. <https://doi.org/10.3390/w14132000>

Academic Editor: Maria Mimikou

Received: 12 May 2022

Accepted: 20 June 2022

Published: 22 June 2022

Publisher's Note: MDPI stays neutral with regard to jurisdictional claims in published maps and institutional affiliations.



Copyright: © 2022 by the authors. Licensee MDPI, Basel, Switzerland. This article is an open access article distributed under the terms and conditions of the Creative Commons Attribution (CC BY) license (<https://creativecommons.org/licenses/by/4.0/>).

1. Introduction

During the past few decades, rapid urbanization has led to major transformations in population size, urban areas, economic development, and social characteristics [1]. With these profound transformations, extreme urban flood events have occurred more frequently, resulting in a growing population exposed to flood hazards and increasing flood damages to human communities [2–7]. There is also spatial heterogeneity in the affected population and economic losses across nations, regions, and communities [8–10]. Certain groups are found to be more vulnerable to flood hazards due to a higher exposure, a lack of access to necessary resources or a lower recovering capacity [11,12]. Hence, it is critical to understand how flood hazards affect different social groups. Urban flood risk assessment has emerged and served as a powerful analytic tool to evaluate the impacts from floods, which could be further applied to guide the reduction of flood risk.

In urban flood risk assessment, flood risk mapping is an important step to the planning of appropriate flood mitigation measures and preparedness of mitigation strategies for different stakeholders. Traditional urban flood risk mapping uses hydrologic modeling to calculate the excess runoff and compute the inundation extent and depth by a 1D-2D hydrodynamic model such as SWMM [13,14], MIKE FLOOD [15] and HEC-RAS [16,17]. More recently, machine learning algorithms have been applied into flood risk mapping and demonstrated a good performance in predicting flood-prone areas [18,19]. However, traditional physically-based models and machine learning methods lack assessment of social factors' impacts on flood risk. On the other hand, the GIS-Based Spatial Multi-Criteria Analysis (SMCA) approach considers both physical and social factors [20,21].

In this framework, disaster risk is viewed as a function of hazard (e.g., flood extent, inundation depth), exposure (e.g., assets and population at risk), and vulnerability (e.g., society's capacity to deal with the potential damage) [7,9,22,23].

As one of the key components in the SMCA framework, the exposure to flooding at urban areas is increasing, due to the general trend of growing urban area and urban population [24,25]. The total amount of urban areas exposed to floods increased by six times during the 20th century and the trend is continuing in the 21st century [26]. In addition, critical infrastructures in urban areas such as railways, electricity grids, and airports are prone to flood damage. As a result, increasing exposure to urban flood can lead to serious consequences including severe economic damages, social disruptions, and loss of lives [27].

Vulnerability is another driver of the increasing flood risk, as it reflects how people experience hazard differently though they are exposed to the same magnitude of flooding [28]. According to Turner et al. [29], vulnerability refers to the degree to which a system is likely to experience harm due to exposure to a hazard. Numerous studies have highlighted that the flood vulnerability is multidimensional [4,5,30–33] and could be classified into several categories, including physical vulnerability [34–37], social vulnerability [12,28,36,38,39], economic vulnerability [30,35], and environmental vulnerability [40]. Commonly used vulnerability assessment methods include principal component analysis (PCA), which enables scientists to identify underlying components from a wide range of vulnerability indicators [9,38,41], and multi-criteria analysis method in which several key indicators are selected and weighted to derive a composite vulnerability index [23,42]. Szewrański et al. [43] developed a Pluvial Flood Risk Tool (PFRA) incorporating hazard, exposure, and vulnerability, but their focus was on the physical impacts of urban fluvial flooding and social impacts were not fully considered. Apel et al. [44] used a complex 2-D hydrodynamic model to develop flood hazard map combining both fluvial and pluvial flood, but they did not evaluate the social factors affecting flood risk.

In order to evaluate urban pluvial flood risk with consideration of both physical and social factors, this work is focused on combining the assessment of physical exposure and social vulnerability at catchment level. The exposure index incorporates the topographic control index (TCI) [45] and impervious area ratio. The social vulnerability index measures how communities are affected differently by urban flood based on their demographic, socioeconomic, and housing conditions. Furthermore, we also explored the interplay impacts of physical exposure and social vulnerability and discussed different urban pluvial flood risk mitigation strategies accordingly. Our catchment-based assessment method can provide a comprehensive understanding of urban pluvial flooding.

The rest of this paper is organized as follows. Section 2 describes the methodology of the study, including the study area, physical exposure assessment, social vulnerability assessment, and composite framework. Section 3 presents the assessment results of flood risk indices. Then, the different flood mitigation strategies according to the flood risk assessment results are discussed in Section 4. In Section 5, general conclusions and recommendations for future research are presented.

2. Methodology

2.1. Study Area

Cincinnati (39.10° N, 84.51° W) is a major city in Ohio, U.S. The city is set on the north bank of the Ohio River and spreads out on hills, with a continental climate producing a wide range of temperatures from winter to summer and an average elevation 224 m. The annual average temperature is 11.83 °C and average annual precipitation is 1019.6 mm. The hottest month is July with an average temperature of 29.8 °C, and the coldest month is January with an average temperature of −5 °C. There are 2.2 million people living in Cincinnati metropolitan area. For the consideration of terrain continuity, City of Norwood and St. Bernard, which are two enclaves, are also included in our study area (Figure 1).

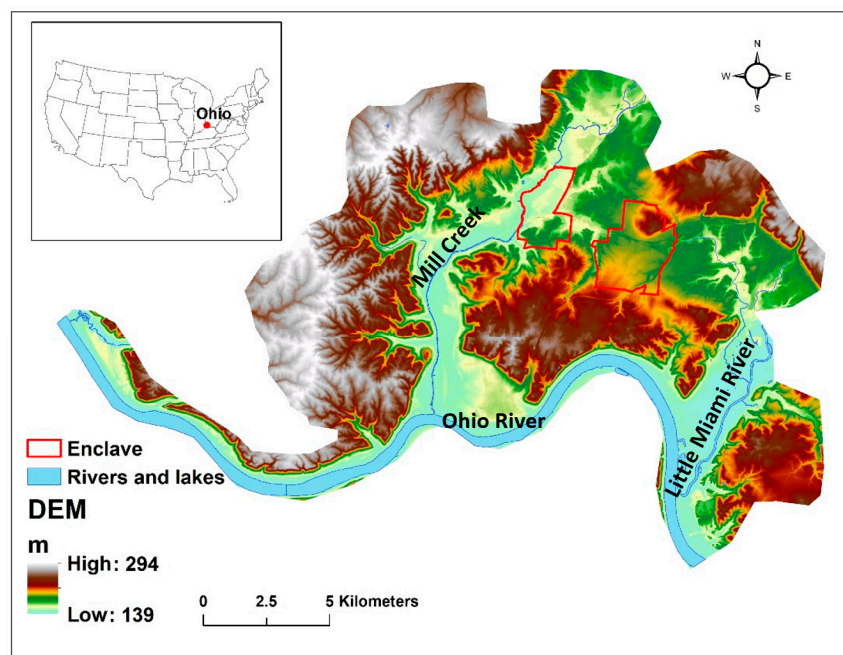


Figure 1. Location map of the study area.

Cincinnati has an infamous history of flooding [46,47], and associated problems of combined sewer overflows (CSOs) [48]. A number of major flood events have been recorded by National Weather Service since 1999. For instance, on 28 August 2016, a once in a 100-year storm caused 76.2 mm rainfall in two hours, causing extensive inundations and severe damages to the neighborhoods in the Cincinnati area.

2.2. Urban Pluvial Flooding Assessment Framework

Urban pluvial flooding differs from other types of flooding, e.g., riverine flooding, coastal flooding in that it occurs at smaller spatial and temporal scales [49]. Pluvial floods can happen anywhere in urban areas and are hard to predict due to its complexity in urban context [50]. Various physical factors, such as micro-topography, climate, land use, and soil conditions, will affect the extent to which population and economic assets are exposed to floods [51–53].

Our conceptual flood risk assessment framework is shown in Figure 2. Heavy rainfall can lead to potential urban pluvial flood risk which is further affected by geographical context of the area (e.g., topography, land cover) and social fabric (e.g., people's living experiences, risk perceptions, built environment). To measure the two aspects of urban pluvial flood risk, a physical exposure index (EI) and a social vulnerability index (SoVI) were developed respectively and then used to compute composite urban pluvial flooding risk index (PFRI). With the understanding of impacts from the different combinations of EI and SoVI, different strategies can be developed accordingly to mitigate flood risk.

2.3. Physical Exposure Assessment

In this study, we selected two indicators, topographic control index (TCI) and impervious area ratio, to measure the exposure to urban pluvial flooding. Topographic elements such as slope, contributing area, and the volumes of depressions are key factors which significantly influence the flow direction and velocity of runoff, and therefore determine the potential places where the pluvial flooding can occur. TCI was initially developed by Huang et al. [52]. It is a depression-based index that integrates topographic elements to evaluate flooding risk for each depression. A larger TCI value means a higher risk for the depression to be inundated in high intensity rainfall events, resulting in a higher exposure to urban flooding. The TCI has been successfully applied to detect frequently flooded urban

areas [52], to map the spatial heterogeneity of pluvial flooding’s controlling factors [45], and to analyze the stability of transmission towers [54]. The TCI in this study was calculated by using a 1.514-m (5 feet) DEM, which was converted from LiDAR data provided by Ohio Geographically Reference Information Program. We calculated the area-weighted TCI values for all the depression catchments in the study area, which includes both depression and its corresponding contributing area. For more detailed information related to the TCI, please refer to our previous research [45].

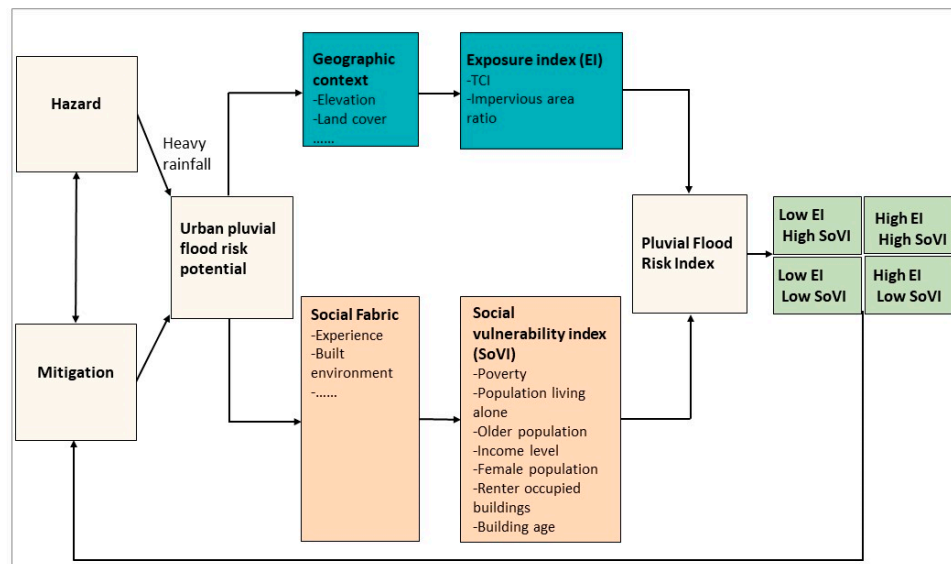


Figure 2. Urban pluvial flood risk assessment framework.

The relationship between impervious surface conditions and potential flooding risk has been emphasized by many studies [55,56]. Increased impervious area will lead to a higher potential flooding risk, as it will lead to poor infiltration, higher runoff peaks, and larger total runoff volume. In this study, we calculated the ratio of impervious surface area over the catchment area for each depression catchment. The land cover geodatabase with impervious area information was downloaded from Cincinnati Area Geographic Information System (CAGIS).

Furthermore, for the validation purpose, we also collect observed flooded locations in four major rainfall events, including the event on 28 August 2016, 12 February 2019, 2 May 2019, and 7 July 2020. There is a total of 47 reported records from local news and social media. We mapped the flooded locations to examine whether they are located in areas with higher values of exposure index as a proxy of validation. Moreover, to explore how rainfall intensity may affect the flooded locations and its relationship with exposure level and social vulnerability, we summarized the normalized rainfall values of the flooded locations, which were calculated as the ratio of the rainfall depth of the flooded location over the maximum rainfall depth in that rainfall event.

2.4. Social Vulnerability Assessment

Social vulnerability, which would affect to what extent communities are disturbed to the natural hazard and how they can cope and adapt to the hazards [28], is related to demographic, social, cultural, and economic conditions of the communities. This term helps to explain why some communities experience a hazard differently, even though they are affected by the same magnitude hazard event. Rufat et al. [57] identified seven theoretical indicators of social vulnerability through a review of 67 flood disaster case studies (1997–2013) related to social vulnerability to floods, and they found that demographic characteristics (e.g., age, race, gender) and socio-economic status (e.g., income, wealth) were the most frequently used indicators of social vulnerability to flooding. There

is no consensus on how the social vulnerability should be measured. In general, social vulnerability is dependent on spatial scale, the local and regional social environment, the data availability of demographic information, and data resolution.

In this study, the data we used for calculating social vulnerability index were collected from American Community Survey (ACS) 5-year estimate for 2014–2018. Following the work by Cutter et al. [19] and previous literature, the social vulnerability index was measured based on seven social vulnerability indicators: (1) percentage of households below poverty level; (2) percentage of households with one or more people 60 years old and over; (3) percentage of households with income lower than \$100,000; (4) percentage of female population; (5) percentage of population living alone; (6) percentage of renter occupied units; and (7) percentage of buildings built before 1939 or earlier. To briefly explain our rationale of indicator selection, poverty level and household income level would affect the ability of a household to cope and adapt to the flooding damage. Female population, older population, and population living alone measures who might be more prone to flooding risk. Compared to homeowners who might have a better knowledge of flood history of the local area as well as a desire to improve their properties by purchasing flooding insurance or flood protection facilities, renters might be more vulnerable to flood damages. Most of the variables were collected at block group level, except for the renter information and household income data which was only available at census tract level. Considering that the data might be sensitive to the area of census block group or census tract, all the indicators used percent variables. The descriptions of vulnerability variables are shown in Table 1.

Table 1. The explanation of urban pluvial flood risk variables.

Risk Component	Variables	Reference
Exposure	TCI	Huang et al. (2019) [52], Qi et al. (2020) [45]
	Impervious area ratio	Qi et al. (2020) [45]
Social vulnerability	% households below poverty level	Cutter et al. (2013) [28]
	% households with one or more people 60 years old and over	Cutter et al. (2013) [28]
	% households with income lower than \$100,000	Cutter et al. (2013) [28]
	% female population	Cutter et al. (2013) [28]
	% population living alone	Ka'zmierzak and Cavan (2011) [9]
	% renter occupied units	Cutter et al. (2013) [28]
	% buildings before 1939 or earlier	Fedeski and Gwilliam (2007) [58]

For the conformity of the unit with physical exposure indicators, all the social vulnerability indicators were aggregated to the catchment level. Moreover, for the validation purpose, we also collected social vulnerability score provided by National Risk Index dataset, which is published in 2020 by FEMA (Federal Emergency Management Agency) from the U.S. government [59]. In the national risk index, social vulnerability score measures the susceptibility of social groups to the adverse impacts of natural hazards. It is calculated based on 29 socio-economic variables using the methodology from Cutter et al. [32]. It is similar to the social vulnerability context in our study. Therefore, we use it to validate the social vulnerability index results in our paper.

2.5. Composite Pluvial Flooding Risk Index

2.5.1. Normalization of Exposure Index and Social Vulnerability Index

All the selected variables (Table 1) were normalized using minimum-maximum normalization method with values ranging from 0 to 1 [60]. The closer to 1, the higher exposure or social vulnerability to urban pluvial floods, and vice versa. As all variables are positively correlated with vulnerability, the standard value for each variable was calculated using Equation (1).

$$X_{ij} = \frac{x_{ij} - \min x_i}{\max x_i - \min x_i}, \quad i = 1, 2, \dots; j = 1, 2, \dots, 9, \quad (1)$$

where X_{ij} are the normalized values of the physical exposure and social vulnerability indicators, x_{ij} is the original value of the indicator.

After normalization, EI and $SoVI$ can be calculated by combining all the exposure/social vulnerability indices with equal weights, respectively. The EI and $SoVI$ are computed as the arithmetic mean of the indicators in Equations (2) and (3).

$$EI = \frac{\sum_{j=1}^2 x_{ij}}{2}, i = 1, 2 \quad (2)$$

$$SoVI = \frac{\sum_{j=1}^7 x_{ij}}{7}, i = 1, 2, \dots, 7 \quad (3)$$

2.5.2. Pluvial Flood Risk Index

Different approaches from other researchers have been applied to integrate different components of flood risk. The common approaches to integrating different dimensions or components of flood risk include linear combination [60–62] and multiplication approach [63,64]. For example, Lyu et al. [65] developed a flood risk model by using linear combination of hazard, exposure, and vulnerability to evaluate flood risk for metro systems. Hazarika et al. [66] evaluated comprehensive flood risk by multiplying hazard by vulnerability and mapped flood hazard zones in Upper Brahmaputra River floodplains.

In this study, a new composite PFRI was computed by multiplying EI with $SoVI$. The rationality behind is that the zero exposure to flooding would have overall the lowest risk no matter how high the social vulnerability is. Similar thoughts can be seen in Szewrański et al. [43] when they calculated the composite risk score by using multiplication method, exposure parameter was assigned zero value for areas that are unlikely to be flooded. The composite PFRI is defined in Equation (4).

$$PFRI = EI * SoVI \quad (4)$$

3. Results

3.1. Exposure to Pluvial Flooding

The TCI and impervious area ratio are classified based on standard deviation (SD) classification method (Figure 3). About 1107 depressions and their corresponding upslope-contributing areas are identified. Generally, depressions are widely distributed in the study area. It can be observed that the majority of the catchments have low TC values, indicating that they have a low exposure to urban pluvial flooding due to unfavorable topographic impacts. Catchments with higher TCI values are mainly located along the riverside of Mill Creek and north part of the study area. Regarding the impervious area ratio, high values are mainly distributed in downtown area and major commercial centers in Cincinnati. Large amount of imperviousness can slow down the infiltration rate and increase runoff volume, resulting in a higher level of exposure to urban pluvial flooding.

Based on the values of TCI and impervious area ratio, the exposure index (EI) was mapped using the SD classification method (Figure 4). Areas with high EI s are mainly located along the riverside of the Mill Creek and Ohio river as well as the north part of the city. We classified the EI values into three groups. Those catchments with EI values higher than 0.5 standard deviations are grouped as high level; -0.5 – 0.5 standard deviations indicate medium level; and areas lower than -0.5 standard deviations are in low level [41]. We then summarized the number and area of the depression catchments based on the three groups of EI values (Table 2). Within the 47 reported flooded locations, 31 flooded locations belong to medium exposure level ($0.15 \leq EI < 0.28$); 14 flooded locations in high exposure level ($0.28 < EI \leq 0.61$); and only 2 flooded locations in low exposure level ($EI < 0.15$).

The reason why many flooded locations belong to medium level is that the catchment areas with medium exposure level is more than two times of the areas with high exposure level. The majority of the catchments have low exposure level, but only two reported flooded locations fall in low exposure level. The 47 reported inundations are located in 18 depression catchments. When comparing the EI values of the 18 flooded catchments with all the depression catchments, we find that the median EI value for flooded catchments is higher, and the flooded catchments have a narrower interquartile range (Figure 5). These results show a high consistency between actual flooded areas and areas with high EIs, which demonstrates the effectiveness of TCI and impervious area ratio in measuring exposure level to urban pluvial flooding. Furthermore, we also summarized the mean normalized rainfall of each flooded location (Table 2), it was calculated by the rainfall amount of the flooded location divided by the maximum rainfall in that rainfall event, so that we can measure the relative rainfall intensity in the range from 0 to 1 for each flooded location in the four rainfall events, for more details, please refer to Qi et al. [45]. The results show that the flooded areas with medium and high exposure levels also have relatively higher levels of rainfall, indicating that the flood risks in the study area are magnified by the positive correlation between EI level and rainfall intensity.

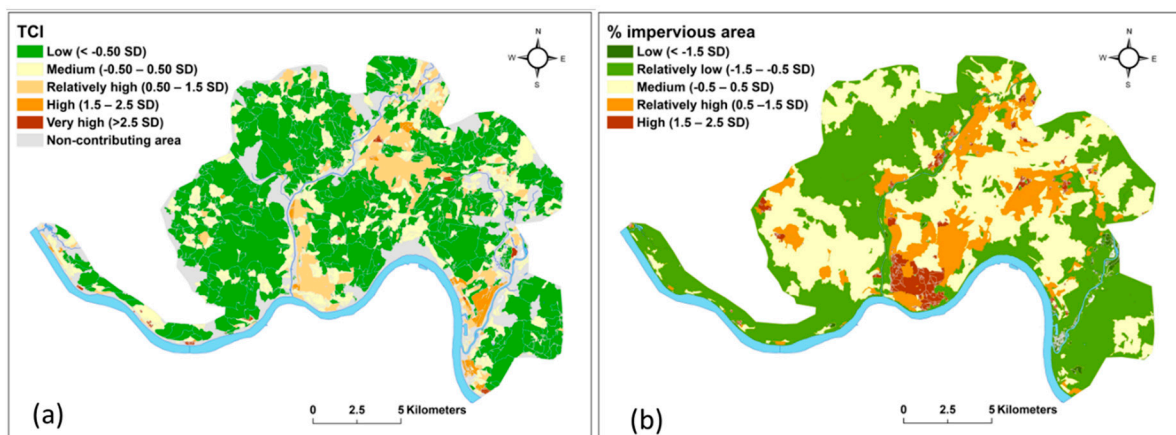


Figure 3. Results of TCI (a) and impervious area ratio (b).

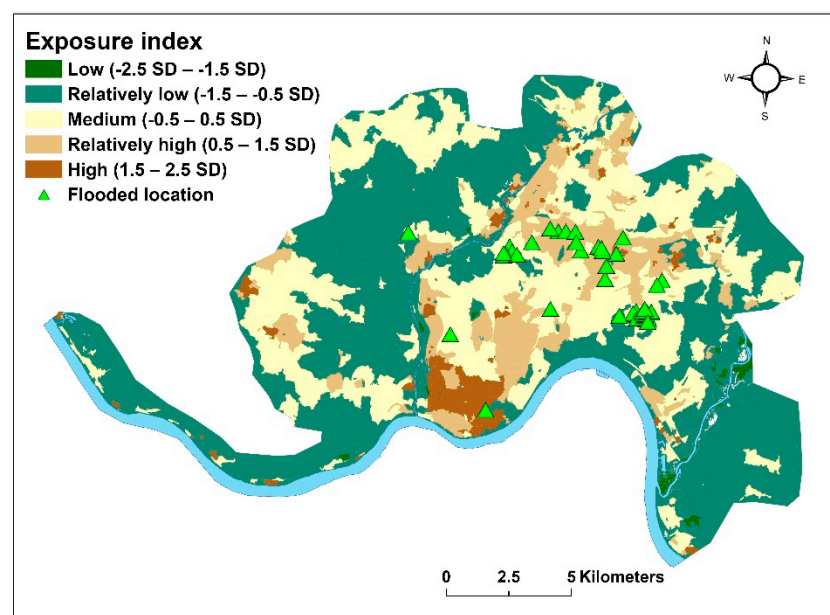


Figure 4. Exposure index.

Table 2. Summary of exposure index (EI) of flooded locations based on EI level.

Exposure Level	EI Range	Area (km ²) (Number of Catchments)	Number of Flooded Locations	Mean Normalized Rainfall
Low	$0 < EI < 0.15$	138.16 (383)	2	0.58
Medium	$0.15 \leq EI < 0.28$	87.44 (411)	31	0.71
High	$0.28 \leq EI < 0.61$	41.86 (313)	14	0.77

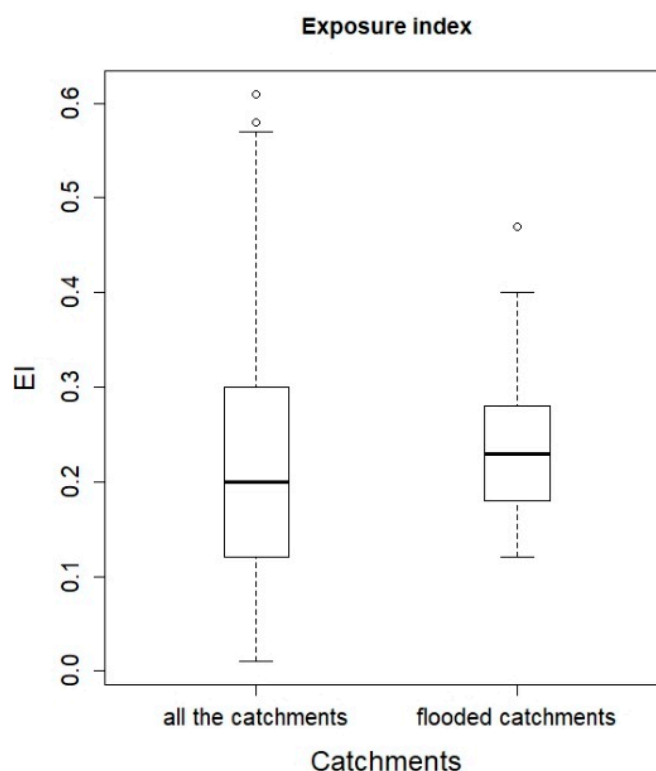


Figure 5. Boxplot of the EI values for all the catchments and flooded catchments.

3.2. Social Vulnerability

Seven social vulnerability indicators were classified based on the SD classification method (Figure 6). It can be observed that the different aspects of social vulnerability are not uniform and large spatial differences can be found in the Cincinnati area. Notably, Cincinnati has a relatively large area with older buildings, which may be adversely affected when hazardous floods happen. There is a relatively high proportion of population living alone in urban centers. Furthermore, in the more built-up urban centers, there is also a high proportion of households that are below poverty level and have a lower income, which may lead to a low capacity for them to adapt to the potential damage caused by urban pluvial flooding. In addition, renters also tend to occupy housing units in urban centers, because there are more job opportunities in commercial districts and living near urban centers can reduce commuting costs. However, they may have higher social vulnerability due to a lack of knowledge about the flooding history of their living area and lower willingness to pay for flood protection costs. On the other hand, older population prefers to live in suburbs in the north part of the city.

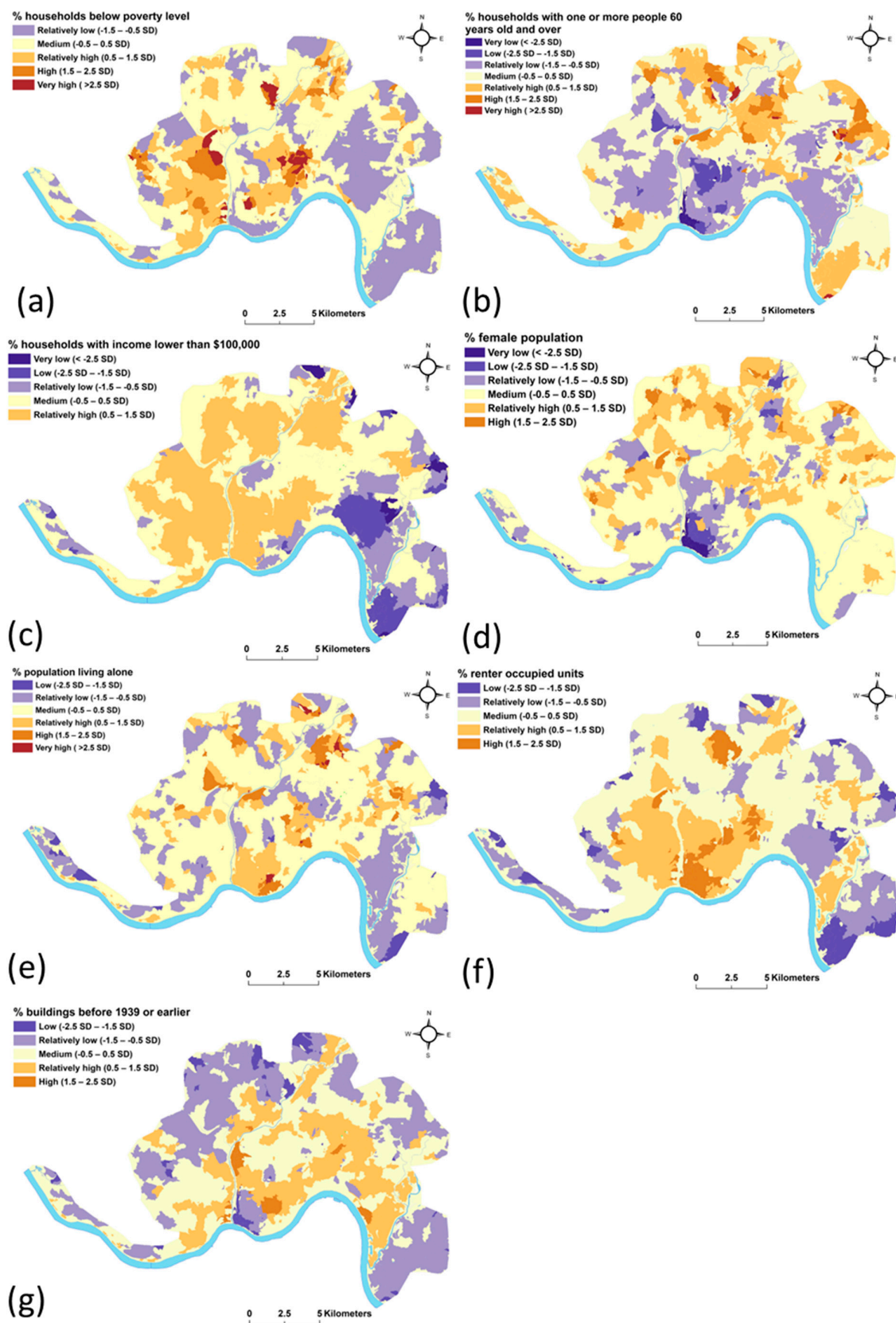


Figure 6. The results of individual social vulnerability indicators, (a) % households below poverty level, (b) % households with one or more people 60 years old and over, (c) % households with income lower than \$100,000, (d) % female population, (e) % population living alone, (f) % renter occupied units, (g) % buildings before 1939 or earlier.

The results of the composite social vulnerability at catchment level are shown in Figure 7 and Table 3. We can see the spatial heterogeneity of the catchments' composite social vulnerability values. High social vulnerability values can be found in the urban center and along the riverside of Mill Creek. The high social vulnerability in these areas is due to a higher proportion of households with lower income and below poverty level, larger population living alone, and more renter occupied housing units. In terms of the reported flooded locations (Table 3), 22 out of 47 flood locations are distributed in catchments with low SoVI values, followed by 16 locations with medium SoVI values, and 9 locations with high SoVI values. We also compared the SoVI values between 18 flooded catchments and all the catchments in the boxplot (Figure 8). Interestingly, the flooded catchments have a slightly lower median SoVI, but there are no significant differences of SoVI values between flooded catchments and all the catchments.

For validation purposes, we aggregated SoVI scores from National Risk Index to catchment level to make it comparable with our calculations of SoVI. The relationship between normalized SoVI scores from NRI dataset and our calculations is shown in Figure 7b. A clear positive correlation can be observed with a relatively good fit ($R^2 = 0.45$, $p < 0.05$), indicating that our social vulnerability indicators are reliable in reflecting the social vulnerability to urban pluvial flooding in the study area.

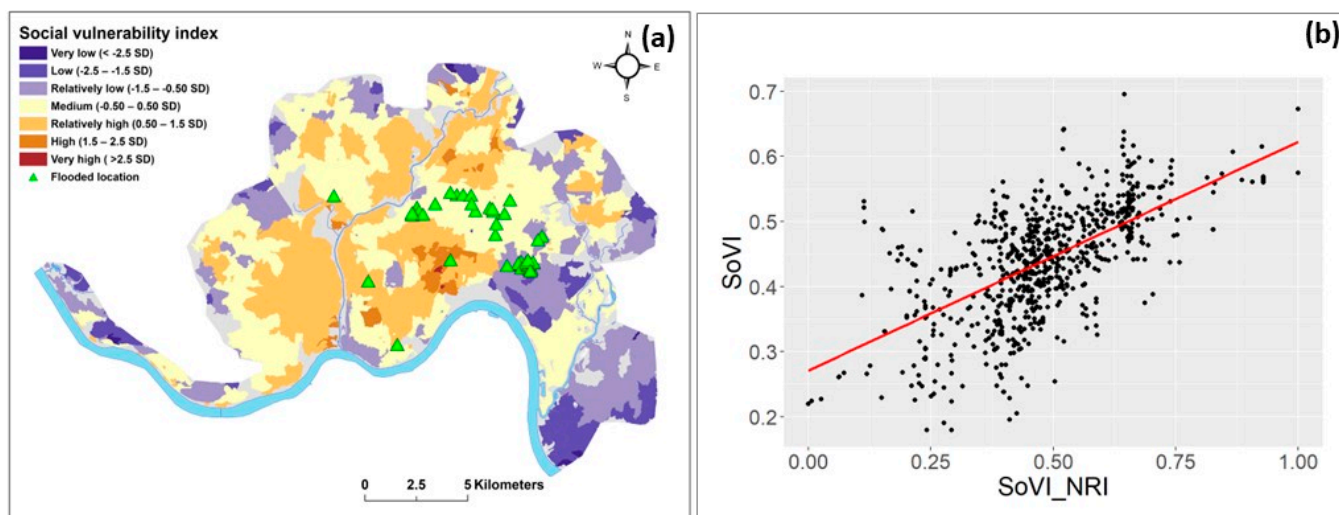


Figure 7. Results of SoVI at catchment level (a) and the relationship between aggregated SoVI score from NRI dataset and our calculations of SoVI (b).

Table 3. Summary of SoVI values of flooded locations based on SoVI level.

SoVI Level	SoVI Range	Area (km ²) (Number of Catchments)	Number of Flooded Locations
Low	0 < SoVI < 0.40	66.28 (308)	22
Medium	0.40 ≤ SoVI < 0.48	127.38 (409)	16
High	0.48 ≤ SoVI < 0.70	73.81 (390)	9

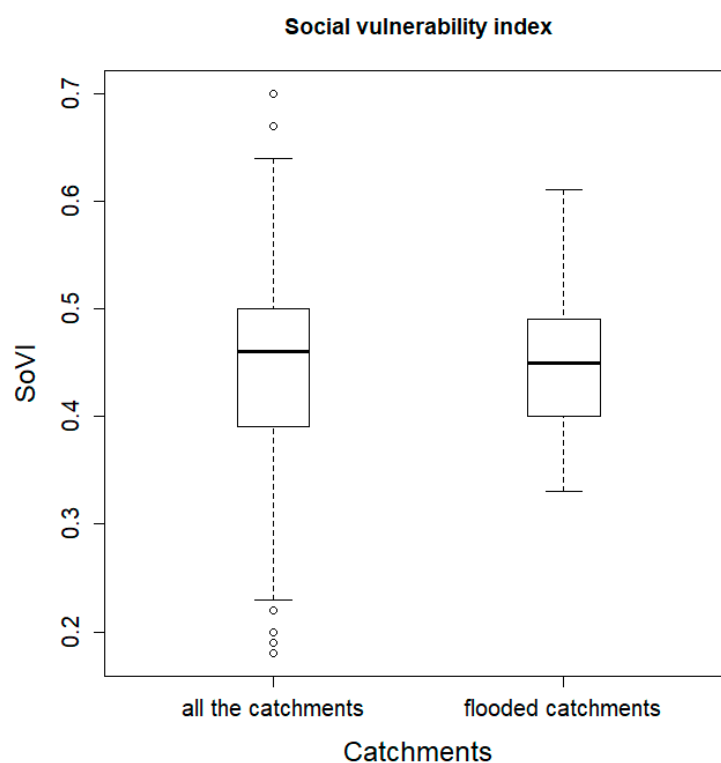


Figure 8. Boxplot of the SoVI values for all the catchments and flooded catchments.

3.3. Urban Pluvial Flood Risk Index

The composite pluvial risk index was calculated and the results are shown in Figure 9. In this map, we also overlaid the observed flooded locations from four rainfall events to examine whether the areas with relatively high composite risk values match with the reality. Generally, the majority of city has a low to medium composite risk to urban pluvial flooding. High composite risk values can be found in the urban center, the riverside of Mill Creek, and the north part of the Cincinnati area. As shown in Table 4, 32 out of 47 flooded locations are in catchments with medium PFRI values ($0.07 < \text{PFRI} \leq 0.13$), followed by 14 flooded locations in catchments with high PFRI values ($0.13 < \text{PFRI} \leq 0.31$), and only one flooded location is in the catchment with low PFRI value ($0 < \text{PFRI} \leq 0.07$). The flooded location with low composite risk has a mean normalized rainfall of 0.72, indicating that the flooding here was largely driven by high rainfall intensity. We also compared the PFRI values between flooded catchments and all the catchments in a boxplot (Figure 10), the median value of PFRI for the flooded catchments is higher and the interquartile range is narrower. Therefore, PFRI values can effectively differentiate depression catchments with higher flood risks from others.

Table 4. Summary of PFRI values for the flooded locations based on PFRI level.

Risk Level	PFRI Range	Area (km ²) (Number of Catchments)	Number of Flooded Locations	Mean Normalized Rainfall
Low	$0 < \text{PFRI} \leq 0.07$	137.12 (404)	1	0.72
Medium	$0.07 < \text{PFRI} \leq 0.13$	88.92 (390)	32	0.70
High	$0.13 < \text{PFRI} < 0.31$	41.44 (313)	14	0.77

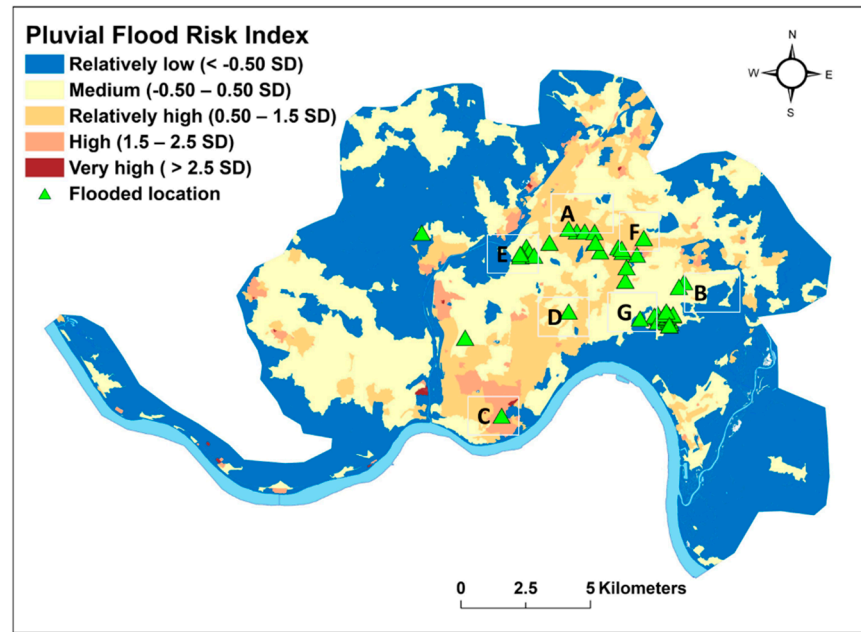


Figure 9. The results of pluvial flood risk index (PFRI).

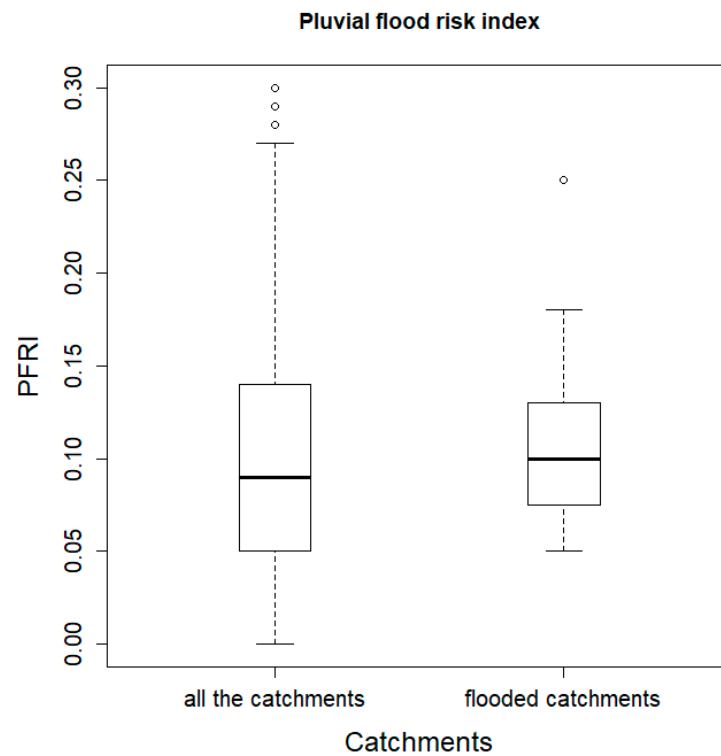


Figure 10. Boxplot of the PFRI values for all the catchments and the flooded catchments.

3.4. Case Analysis

To examine how the composite risk is affected by its two components, we selected seven catchments which included flooded locations to conduct further analysis (Figure 9, Table 5). We also added the mean normalized rainfall for each catchment into the discussion. Clearly, the catchments demonstrate interplay of the impacts from two aspects of urban pluvial flooding risk and rainfall intensity.

For Catchment A, it has relatively high physical exposure and medium social vulnerability, resulting in a relatively high composite risk. Similar patterns can be observed from Catchment F. Catchment A is characterized by high TCI value due to a very large contributing area and a relatively high proportion of impervious area. Moreover, high rainfall intensity also contributes to its high pluvial flood risk. This area was reported to be seriously affected by flooding on 28 August 2016, multiple roads and schools were closed due to high water levels. With regard to Catchment C, its high composite risk to urban pluvial flooding is driven by high physical exposure and relatively high social vulnerability. Dual impacts from physical environmental setting such as unfavorable topography and high imperviousness as well as socioeconomic factors such as lower income and renter occupied units make the communities even more vulnerable to urban pluvial flooding. By contrast, Catchment G has both relatively low exposure level and social vulnerability, leading to a relatively low composite risk. The inundation is largely driven by high intensity rainfall. Although catchments B, D, and E have similar exposure level and composite risk level, the pattern of social vulnerability level varies. Catchments D and E have high and relatively high social vulnerability while Catchment B has relatively low social vulnerability. In other words, communities in Catchment D and E may be more vulnerable to flood damage when hazardous flood events happen. From the analysis above, we can conclude that the spatial heterogeneity of the impacts and the interplay of the two components of pluvial flood risk can either exacerbate or alleviate the communities' risk to urban pluvial flooding.

Table 5. Summary of the case analysis of seven flooded catchments.

Catchment	EI	SoVI	PFRI	Mean Normalized Rainfall	Pattern Description
A	0.28	0.48	0.14	0.77	High EI, Medium SoVI
B	0.23	0.34	0.08	0.75	Medium EI, Low SoVI
C	0.47	0.53	0.25	0.62	High EI, High SoVI
D	0.18	0.57	0.11	0.76	Medium EI, High SoVI
E	0.18	0.50	0.09	0.50	Medium EI, High SoVI
F	0.30	0.46	0.14	0.89	High EI, Medium SoVI
G	0.14	0.38	0.05	0.72	Low EI, Low SoVI

4. Discussion

4.1. Catchment-Based Approach for Urban Pluvial Flooding Risk and Vulnerability Assessment

This study presents an approach to assess the pluvial flooding risk by combining exposure and social vulnerability at catchment scale. Furthermore, we also validate the exposure assessment by examining the consistency between EI values and observed flooded locations. The validation results reported that 95% of the flooded areas are located in the catchments with medium and high exposure levels. The results can provide useful insights for pluvial flooding risk management at catchment level. The catchment perspective in understanding the flooding process was also highlighted by Garner et al. [67], and physical catchment properties (e.g., area, geology, land use) are closely related to flood generating process. Small catchments tend to be more vulnerable to human impacts due to a lack of established flooding defense and enhanced individual exposure [68,69]. Thus, current flood hazard-related studies call for a catchment perspective in urban flooding risk research. Our catchment-based approach for urban pluvial flooding risk assessment can help to provide a whole picture of urban pluvial flooding risk for policymakers in formulating effective flood mitigation strategies.

Our exposure assessment to urban pluvial flooding can quantify how physical characteristics such slope, area, and land cover affect population's exposure to urban pluvial flooding through the two indicators, topographic control index (TCI) and impervious area ratio. It was demonstrated in our study that the TCI can serve as a useful indicator to identify the flood prone areas for urban planners, policymakers, and other researchers, this result is also in accordance with Huang et al. [52], in their case study in Guangzhou,

China. In addition, our study identified the spatial clustering of exposure to flooding. Similar spatial clustering patterns of high exposure are also observed by Pricope et al. [41], which reported that there is a proportion of 27% block groups with high flood exposure in their study area. Our assessment of social vulnerability is comparable to other studies as well, which highlighted socioeconomic characteristics such as income, poverty, age, gender, housing [12,28,31]. These social factors will affect population's vulnerability to urban flooding at varying levels, which demonstrates the need to enhance communities' adaptive capacity to urban flooding, especially for certain vulnerable groups such as poor communities or older communities.

4.2. Flooding Mitigation Implications Based on Different Combinations of Risk Components

The physical exposure and social vulnerability reflect different aspects of urban pluvial flooding risk. Physical risk of urban flooding can be mitigated by applying low impact development techniques such as rainfall gardens, permeable pavement, green roofs, as well as more efficient urban drainage systems [70–74]. Social vulnerability can be mitigated by providing affordable flood insurance or loans for certain vulnerable groups and building flood shelters to help them to adapt and recover from urban flooding [23,75,76]. As shown in previous analysis, there are four possible combinations of physical exposure and social vulnerability, namely, high exposure and high social vulnerability, high exposure and low social vulnerability, low exposure and high social vulnerability and low exposure and low social vulnerability (Figure 11). In this study, high exposure/high social vulnerability catchments were defined as the catchments with EI/SoVI values higher than 0.5 standard deviations respectively. Similarly, catchments with low exposure or low social vulnerability were defined as the catchments with EI/SoVI values below 0.5 standard deviations respectively. As our results suggest, the interplay of these two components can either exacerbate or alleviate the communities' composite risk to urban flooding. Therefore, the different combinations of physical exposure and social vulnerability to urban pluvial flooding would have different implications for flood mitigation measures. The areas with both high exposure and social vulnerability to urban pluvial flooding should be given the highest priority in flood mitigation management. In these high-risk areas, flood mitigation measures aimed at both physical side and social side of flood risk should be developed. For areas with high exposure and low social vulnerability, the focus of flood mitigation measure should be attenuating the physical risk of urban flooding. In terms of the areas with low physical exposure and high social vulnerability, the flood mitigation strategy should be more focused on the community adaptability and readiness to urban floods.

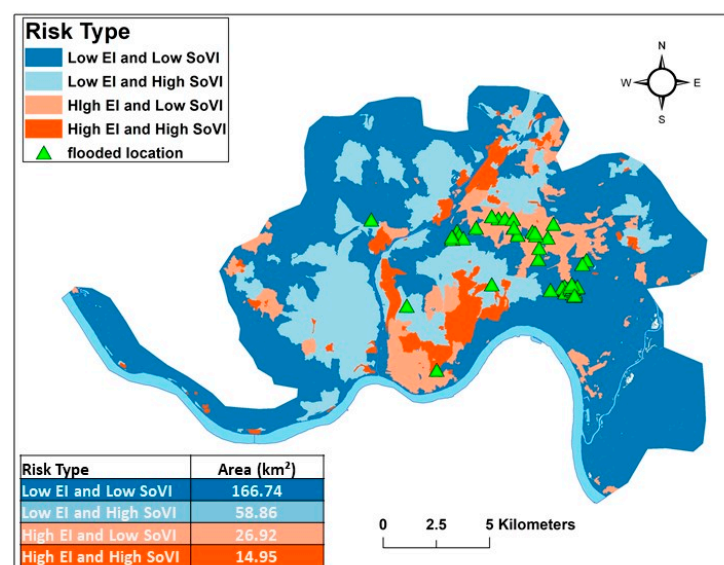


Figure 11. Risk type of urban pluvial flooding.

5. Conclusions

This paper investigates spatial patterns of urban pluvial flooding risk by integrating the two components of risk including physical exposure and social vulnerability at catchment level in the City of Cincinnati. The exposure index incorporating impervious area and TCI (topographic control index) can effectively measure to what extent the area is exposed to urban pluvial flood. Social vulnerability index reflects how communities are affected by urban pluvial flood based on their demographic, socioeconomic and housing conditions. The results show that the evaluated composite flood risk has a good match with the historical flooded records. Our catchment-based-on pluvial flood risk investigation can provide useful insights for urban pluvial flooding risk management at catchment level. This method enables us to explore the spatial heterogeneity and interplay impacts of the risk components and risk indicators. While the physical exposure exerts the primary impact, the real impacts can be either exacerbated or alleviated by communities' social vulnerability. We suggest that design of urban flooding mitigation measures should consider both communities' physical exposure and social vulnerability to urban pluvial flooding, specifically, those areas with both high exposure and high social vulnerability are of the highest priority. The areas with high exposure but low social vulnerability are secondary, and the focus is on mitigating the exposure to urban pluvial flooding. Our methodology of integrated assessment of urban pluvial flooding risk and discussions on the interplay impacts of physical exposure and social vulnerability can provide a comprehensive understanding of urban pluvial flooding risk and promote the formulation of effective flood mitigation strategies for the government and policymakers. One of the limitations of our study is that we only focused on the pluvial flood while ignoring fluvial flood in this study, future work may combine both pluvial flood and fluvial flood in urban flood risk evaluation.

Author Contributions: Conceptualization, X.C.; methodology, M.Q.; formal analysis, M.Q.; investigation, M.Q.; data curation, M.Q.; writing—original draft preparation, M.Q. and X.C.; writing—review and editing, X.C., H.H. and L.L.; visualization, M.Q.; supervision, X.C.; project administration, X.C. All authors have read and agreed to the published version of the manuscript.

Funding: This research was partly funded by City of Cincinnati, Metropolitan Sewer District (Grant #1018330) and Guangdong Basic and Applied Basic Research Foundation (Grant #2022A1515011494).

Institutional Review Board Statement: Not applicable.

Informed Consent Statement: Not applicable.

Data Availability Statement: The data presented in this study are publicly available at Ohio Geographically Reference Information Program, Cincinnati Area Geographic Information System, American Community Survey, and Federal Emergency Management Agency.

Acknowledgments: The authors thank the Department of Geography and Geographic Information Science, University of Cincinnati for providing software support.

Conflicts of Interest: The funders had no role in the design of the study; in the collection, analyses, or interpretation of data; in the writing of the manuscript, or in the decision to publish the results.

References

1. Cutter, S.L.; Finch, C. Temporal and spatial changes in social vulnerability to natural hazards. *Proc. Natl. Acad. Sci. USA* **2008**, *105*, 2301–2306. [[CrossRef](#)] [[PubMed](#)]
2. Aerts, J.C.J.H.; Botzen, W.J.; Clarke, K.; Cutter, S.L.; Hall, J.W.; Merz, B.; Michel-Kerjan, E.; Mysiak, J.; Surminski, S.; Kunreuther, H. Integrating human behaviour dynamics into flood disaster risk assessment. *Nat. Clim. Chang.* **2018**, *8*, 193–199. [[CrossRef](#)]
3. Jongman, B.; Ward, P.J.; Aerts, J.C.J.H. Global exposure to river and coastal flooding: Long term trends and changes. *Glob. Environ. Chang.* **2012**, *22*, 823–835. [[CrossRef](#)]
4. Balica, S.F.; Douben, N.; Wright, N.G. Flood vulnerability indices at varying spatial scales. *Water Sci. Technol.* **2009**, *60*, 2571–2580. [[CrossRef](#)]
5. Yang, W.; Xu, K.; Lian, J.; Bin, L.; Ma, C. Multiple flood vulnerability assessment approach based on fuzzy comprehensive evaluation method and coordinated development degree model. *J. Environ. Manag.* **2018**, *213*, 440–450. [[CrossRef](#)]

6. Gaume, E.; Bain, V.; Bernardara, P.; Newinger, O.; Barbuc, M.; Bateman, A.; Blaškovičová, L.; Blöschl, G.; Borga, M.; Dumitrescu, A.; et al. A compilation of data on European flash floods. *J. Hydrol.* **2009**, *367*, 70–78. [[CrossRef](#)]
7. Abebe, Y.; Kabir, G.; Tesfamariam, S. Assessing urban areas vulnerability to pluvial flooding using GIS applications and Bayesian Belief Network model. *J. Clean. Prod.* **2018**, *174*, 1629–1641. [[CrossRef](#)]
8. Yoon, D.K. Assessment of social vulnerability to natural disasters: A comparative study. *Nat. Hazards* **2012**, *63*, 823–843. [[CrossRef](#)]
9. Kazmierczak, A.; Cavan, G. Surface water flooding risk to urban communities: Analysis of vulnerability, hazard and exposure. *Landsc. Urban Plan.* **2011**, *103*, 185–197. [[CrossRef](#)]
10. Shah, A.A.; Ye, J.; Abid, M.; Khan, J.; Amir, S.M. Flood hazards: Household vulnerability and resilience in disaster-prone districts of Khyber Pakhtunkhwa province, Pakistan. *Nat. Hazards* **2018**, *93*, 147–165. [[CrossRef](#)]
11. Wu, S.-Y.; Yarnal, B.; Fisher, A. Vulnerability of coastal communities to sea-level rise: A case study of Cape May County, New Jersey, USA. *Clim. Res.* **2002**, *22*, 255–270. [[CrossRef](#)]
12. Felsenstein, D.; Lichter, M. Social and economic vulnerability of coastal communities to sea-level rise and extreme flooding. *Nat. Hazards* **2014**, *71*, 463–491. [[CrossRef](#)]
13. Yang, Y.; Sun, L.; Li, R.; Yin, J.; Yu, D. Linking a Storm Water Management Model to a Novel Two-Dimensional Model for Urban Pluvial Flood Modeling. *Int. J. Disaster Risk Sci.* **2020**, *11*, 508–518. [[CrossRef](#)]
14. Sañudo, E.; Cea, L.; Puertas, J. Modelling Pluvial Flooding in Urban Areas Coupling the Models Iber and SWMM. *Water* **2020**, *12*, 2647. [[CrossRef](#)]
15. Li, W.; Xu, B.; Wen, J. Scenario-based community flood risk assessment: A case study of Taining county town, Fujian province, China. *Nat. Hazards* **2016**, *82*, 193–208. [[CrossRef](#)]
16. Rangari, V.A.; Umamahesh, N.V.; Bhatt, C.M. Assessment of inundation risk in urban floods using HEC RAS 2D. *Model. Earth Syst. Environ.* **2019**, *5*, 1839–1851. [[CrossRef](#)]
17. Mihiu-Pintilie, A.; Cîmpianu, C.I.; Stoleriu, C.C.; Pérez, M.N.; Paveluc, L.E. Using High-Density LiDAR Data and 2D Streamflow Hydraulic Modeling to Improve Urban Flood Hazard Maps: A HEC-RAS Multi-Scenario Approach. *Water* **2019**, *11*, 1832. [[CrossRef](#)]
18. Darabi, H.; Choubin, B.; Rahmati, O.; Haghighi, A.T.; Pradhan, B.; Kløve, B. Urban flood risk mapping using the GARP and QUEST models: A comparative study of machine learning techniques. *J. Hydrol.* **2019**, *569*, 142–154. [[CrossRef](#)]
19. Zhao, G.; Pang, B.; Xu, Z.; Peng, D.; Xu, L. Assessment of urban flood susceptibility using semi-supervised machine learning model. *Sci. Total Environ.* **2019**, *659*, 940–949. [[CrossRef](#)]
20. Hadipour, V.; Vafaie, F.; Deilami, K. Coastal Flooding Risk Assessment Using a GIS-Based Spatial Multi-Criteria Decision Analysis Approach. *Water* **2020**, *12*, 2379. [[CrossRef](#)]
21. Feloni, E.; Mousadis, I.; Baltas, E. Flood vulnerability assessment using a GIS-based multi-criteria approach—The case of Attica region. *J. Flood Risk Manag.* **2020**, *13*, e12563. [[CrossRef](#)]
22. IPCC. Managing the Risks of Extreme Events and Disasters to Advance Climate Change Adaptation. In *A Special Report of Working Groups I and II of the Intergovernmental Panel on Climate Change*; Field, C.B., Barros, V., Stocker, T.F., Qin, D., Dokken, D.J., Ebi, K.L., Mastrandrea, M.D., Mach, K.J., Plattner, G.-K., Allen, S.K., et al., Eds.; Cambridge University Press: Cambridge, UK; New York, NY, USA, 2012; 582p.
23. Koks, E.E.; Jongman, B.; Husby, T.G.; Botzen, W.J.W. Combining hazard, exposure and social vulnerability to provide lessons for flood risk management. *Environ. Sci. Policy* **2015**, *47*, 42–52. [[CrossRef](#)]
24. McGranahan, G.; Balk, D.; Anderson, B. The rising tide: Assessing the risks of climate change and human settlements in low elevation coastal zones. *Environ. Urban.* **2007**, *19*, 17–37. [[CrossRef](#)]
25. Jongman, B.; Hochrainer-Stigler, S.; Feyen, L.; Aerts, J.C.J.H.; Mechler, R.; Botzen, W.J.W.; Bouwer, L.M.; Pflug, G.; Rojas, R.; Ward, P.J. Increasing stress on disaster-risk finance due to large floods. *Nat. Clim. Chang.* **2014**, *4*, 264–268. [[CrossRef](#)]
26. de Moel, H.; Aerts, J.C.; Koomen, E. Development of flood exposure in the Netherlands during the 20th and 21st century. *Glob. Environ. Chang.* **2011**, *21*, 620–627. [[CrossRef](#)]
27. Pant, R.; Thacker, S.; Hall, J.W.; Alderson, D.; Barr, S. Critical infrastructure impact assessment due to flood exposure. *J. Flood Risk Manag.* **2018**, *11*, 22–33. [[CrossRef](#)]
28. Cutter, S.; Emrich, C.; Morath, D.; Dunning, C. Integrating social vulnerability into federal flood risk management planning. *J. Flood Risk Manag.* **2013**, *6*, 332–344. [[CrossRef](#)]
29. Turner, B.L., II; Kasperson, R.E.; Matson, P.A.; McCarthy, J.J.; Corell, R.W.; Christensen, L.; Eckley, N.; Kasperson, J.X.; Luers, A.; Martello, M.L.; et al. A framework for vulnerability analysis in sustainability science. *Proc. Natl. Acad. Sci. USA* **2003**, *100*, 8074–8079. [[CrossRef](#)]
30. Aroca-Jiménez, E.; Bodoque, J.M.; García, J.A.; Díez-Herrero, A. A quantitative methodology for the assessment of the regional economic vulnerability to flash floods. *J. Hydrol.* **2018**, *565*, 386–399. [[CrossRef](#)]
31. Jha, R.K.; Gundimeda, H. An integrated assessment of vulnerability to floods using composite index—A district level analysis for Bihar, India. *Int. J. Disaster Risk Reduct.* **2019**, *35*, 101074. [[CrossRef](#)]
32. Cutter, S.L.; Boruff, B.J.; Shirley, W.L. Social Vulnerability to Environmental Hazards. *Soc. Sci. Q.* **2003**, *84*, 242–261. [[CrossRef](#)]
33. Cutter, S.L.; Mitchell, J.T.; Scott, M.S. Revealing the Vulnerability of People and Places: A Case Study of Georgetown County, South Carolina. *Ann. Assoc. Am. Geogr.* **2000**, *90*, 713–737. [[CrossRef](#)]

34. Karagiorgos, K.; Thaler, T.; Heiser, M.; Hübl, J.; Fuchs, S. Integrated flash flood vulnerability assessment: Insights from East Attica, Greece. *J. Hydrol.* **2016**, *541*, 553–562. [[CrossRef](#)]
35. Rana, I.A.; Routray, J.K. Multidimensional Model for Vulnerability Assessment of Urban Flooding: An Empirical Study in Pakistan. *Int. J. Disaster Risk Sci.* **2018**, *9*, 359–375. [[CrossRef](#)]
36. Rahman, M.T.; Aldosary, A.S.; Nahiduzzaman, K.; Reza, I. Vulnerability of flash flooding in Riyadh, Saudi Arabia. *Nat. Hazards* **2016**, *84*, 1807–1830. [[CrossRef](#)]
37. Nazeer, M.; Bork, H.-R. Flood Vulnerability Assessment through Different Methodological Approaches in the Context of North-West Khyber Pakhtunkhwa, Pakistan. *Sustainability* **2019**, *11*, 6695. [[CrossRef](#)]
38. Zhang, M.; Xiang, W.; Chen, M.; Mao, Z. Measuring Social Vulnerability to Flood Disasters in China. *Sustainability* **2018**, *10*, 2676. [[CrossRef](#)]
39. Fekete, A. Validation of a social vulnerability index in context to river-floods in Germany. *Nat. Hazards Earth Syst. Sci.* **2009**, *9*, 393–403. [[CrossRef](#)]
40. Zachos, L.G.; Swann, C.T.; Altinakar, M.S.; McGrath, M.Z.; Thomas, D. Flood vulnerability indices and emergency management planning in the Yazoo Basin, Mississippi. *Int. J. Disaster Risk Reduct.* **2016**, *18*, 89–99. [[CrossRef](#)]
41. Pricope, N.G.; Halls, J.N.; Rosul, L.M. Modeling residential coastal flood vulnerability using finished-floor elevations and socio-economic characteristics. *J. Environ. Manag.* **2019**, *237*, 387–398. [[CrossRef](#)]
42. Karunarathne, A.Y.; Lee, G. Developing a multi-facet social vulnerability measure for flood disasters at the micro-level assessment. *Int. J. Disaster Risk Reduct.* **2020**, *49*, 101679. [[CrossRef](#)]
43. Szewrański, S.; Chruściński, J.; Kazak, J.; Świader, M.; Tokarczyk-Dorociak, K.; Żmuda, R. Pluvial Flood Risk Assessment Tool (PFRA) for Rainwater Management and Adaptation to Climate Change in Newly Urbanised Areas. *Water* **2018**, *10*, 386. [[CrossRef](#)]
44. Apel, H.; Trepat, O.M.; Hung, N.N.; Chinh, D.T.; Merz, B.; Dung, N.V. Combined fluvial and pluvial urban flood hazard analysis: Concept development and application to Can Tho city, Mekong Delta, Vietnam. *Nat. Hazards Earth Syst. Sci.* **2016**, *16*, 941–961. [[CrossRef](#)]
45. Qi, M.; Huang, H.; Liu, L.; Chen, X. Spatial heterogeneity of controlling factors' impact on urban pluvial flooding in Cincinnati, US. *Appl. Geogr.* **2020**, *125*, 102362. [[CrossRef](#)]
46. Hibbs, A.S. Cincinnati Water Works in the 1937 Flood. *J. Am. Water Work. Assoc.* **1937**, *29*, 1237–1245. [[CrossRef](#)]
47. Cook, A.H. Troubled Waters: Cincinnati's West End and the Great Flood of 1937. *Ohio Val. Hist.* **2007**, *7*, 31–52. Available online: <https://www.musejhu.edu/article/575453> (accessed on 12 November 2021).
48. Fu, X.; Goddard, H.; Wang, X.; Hopton, M.E. Development of a scenario-based stormwater management planning support system for reducing combined sewer overflows (CSOs). *J. Environ. Manag.* **2019**, *236*, 571–580. [[CrossRef](#)]
49. Rözer, V.; Müller, M.; Bubeck, P.; Kienzler, S.; Thieken, A.; Pech, I.; Schröter, K.; Buchholz, O.; Kreibich, H. Coping with Pluvial Floods by Private Households. *Water* **2016**, *8*, 304. [[CrossRef](#)]
50. Grahn, T.; Nyberg, L. Assessment of pluvial flood exposure and vulnerability of residential areas. *Int. J. Disaster Risk Reduct.* **2017**, *21*, 367–375. [[CrossRef](#)]
51. Miller, J.D.; Hutchins, M. The impacts of urbanisation and climate change on urban flooding and urban water quality: A review of the evidence concerning the United Kingdom. *J. Hydrol. Reg. Stud.* **2017**, *12*, 345–362. [[CrossRef](#)]
52. Huang, H.; Chen, X.; Wang, X.; Wang, X.; Liu, L. A Depression-Based Index to Represent Topographic Control in Urban Pluvial Flooding. *Water* **2019**, *11*, 2115. [[CrossRef](#)]
53. Sörensen, J.; Mobini, S. Pluvial, urban flood mechanisms and characteristics—Assessment based on insurance claims. *J. Hydrol.* **2017**, *555*, 51–67. [[CrossRef](#)]
54. Chen, M.; Chan, T.O.; Wang, X.; Luo, M.; Lin, Y.; Huang, H.; Sun, Y.; Cui, G.; Huang, Y. A risk analysis framework for transmission towers under potential pluvial flood-LiDAR survey and geometric modelling. *Int. J. Disaster Risk Reduct.* **2020**, *50*, 101862. [[CrossRef](#)]
55. Huong, H.T.L.; Pathirana, A. Urbanization and climate change impacts on future urban flooding in Can Tho city, Vietnam. *Hydrol. Earth Syst. Sci.* **2013**, *17*, 379–394. [[CrossRef](#)]
56. Shuster, W.D.; Bonta, J.; Thurston, H.; Warnemuende, E.; Smith, D.R. Impacts of impervious surface on watershed hydrology: A review. *Urban Water J.* **2005**, *2*, 263–275. [[CrossRef](#)]
57. Rufat, S.; Tate, E.; Burton, C.G.; Maroof, A.S. Social vulnerability to floods: Review of case studies and implications for measurement. *Int. J. Disaster Risk Reduct.* **2015**, *14*, 470–486. [[CrossRef](#)]
58. Fedeski, M.; Gwilliam, J. Urban sustainability in the presence of flood and geological hazards: The development of a GIS-based vulnerability and risk assessment methodology. *Landsc. Urban Plan.* **2007**, *83*, 50–61. [[CrossRef](#)]
59. Zuzak, C.; Kealey, D.; Goodenough, E.; Stanton, C. *National Risk Index Technical Documentation*; Federal Emergency Management Agency: Washington, DC, USA, 2020. Available online: https://www.fema.gov/sites/default/files/documents/fema_national-risk-index_technical-documentation.pdf (accessed on 12 November 2021).
60. Wang, Y.; Li, Z.; Tang, Z.; Zeng, G. A GIS-Based Spatial Multi-Criteria Approach for Flood Risk Assessment in the Dongting Lake Region, Hunan, Central China. *Water Resour. Manag.* **2011**, *25*, 3465–3484. [[CrossRef](#)]
61. Kubal, C.; Haase, D.; Meyer, V.; Scheuer, S. Integrated urban flood risk assessment—Adapting a multicriteria approach to a city. *Nat. Hazards Earth Syst. Sci.* **2009**, *9*, 1881–1895. [[CrossRef](#)]

62. Zhang, D.; Shi, X.; Xu, H.; Jing, Q.; Pan, X.; Liu, T.; Wang, H.; Hou, H. A GIS-based spatial multi-index model for flood risk assessment in the Yangtze River Basin, China. *Environ. Impact Assess. Rev.* **2020**, *83*, 106397. [[CrossRef](#)]
63. Zhou, Q.; Mikkelsen, P.S.; Halsnæs, K.; Arnbjerg-Nielsen, K. Framework for economic pluvial flood risk assessment considering climate change effects and adaptation benefits. *J. Hydrol.* **2012**, *414–415*, 539–549. [[CrossRef](#)]
64. Lyu, H.-M.; Shen, S.-L.; Zhou, A.-N.; Zhou, W.-H. Flood risk assessment of metro systems in a subsiding environment using the interval FAHP-FCA approach. *Sustain. Cities Soc.* **2019**, *50*, 101682. [[CrossRef](#)]
65. Lyu, H.-M.; Sun, W.; Shen, S.-L.; Arulrajah, A. Flood risk assessment in metro systems of mega-cities using a GIS-based modeling approach. *Sci. Total Environ.* **2018**, *626*, 1012–1025. [[CrossRef](#)] [[PubMed](#)]
66. Hazarika, N.; Barman, D.; Das, A.K.; Sarma, A.K.; Borah, S.B. Assessing and mapping flood hazard, vulnerability and risk in the Upper Brahmaputra River valley using stakeholders' knowledge and multicriteria evaluation (MCE). *J. Flood Risk Manag.* **2018**, *11*, S700–S716. [[CrossRef](#)]
67. Garner, G.; Van Loon, A.F.; Prudhomme, C.; Hannah, D.M. Hydroclimatology of extreme river flows. *Freshw. Biol.* **2015**, *60*, 2461–2476. [[CrossRef](#)]
68. Drobot, S.; Parker, D.J. Advances and challenges in flash flood warnings. *Environ. Hazards* **2007**, *7*, 173–178. [[CrossRef](#)]
69. Špitalar, M.; Gourley, J.J.; Lutoff, C.; Kirstetter, P.-E.; Brilly, M.; Carr, N. Analysis of flash flood parameters and human impacts in the US from 2006 to 2012. *J. Hydrol.* **2014**, *519*, 863–870. [[CrossRef](#)]
70. Hu, M.; Zhang, X.; Li, Y.; Yang, H.; Tanaka, K. Flood mitigation performance of low impact development technologies under different storms for retrofitting an urbanized area. *J. Clean. Prod.* **2019**, *222*, 373–380. [[CrossRef](#)]
71. Lee, J.; Moon, H.; Kim, T.; Kim, H.; Han, M. Quantitative analysis on the urban flood mitigation effect by the extensive green roof system. *Environ. Pollut.* **2013**, *181*, 257–261. [[CrossRef](#)]
72. Ercolani, G.; Chiaradia, E.A.; Gandolfi, C.; Castelli, F.; Masseroni, D. Evaluating performances of green roofs for stormwater runoff mitigation in a high flood risk urban catchment. *J. Hydrol.* **2018**, *566*, 830–845. [[CrossRef](#)]
73. Zhou, Q. A Review of Sustainable Urban Drainage Systems Considering the Climate Change and Urbanization Impacts. *Water* **2014**, *6*, 976–992. [[CrossRef](#)]
74. Ahiablame, L.; Shakya, R. Modeling flood reduction effects of low impact development at a watershed scale. *J. Environ. Manag.* **2016**, *171*, 81–91. [[CrossRef](#)] [[PubMed](#)]
75. Kousky, C. Financing Flood Losses: A Discussion of the National Flood Insurance Program. *Risk Manag. Insur. Rev.* **2018**, *21*, 11–32. [[CrossRef](#)]
76. Thaler, T.; Hartmann, T. Justice and flood risk management: Reflecting on different approaches to distribute and allocate flood risk management in Europe. *Nat. Hazards* **2016**, *83*, 129–147. [[CrossRef](#)]